WIND-DRIVEN RAIN ON HIGH-RISE BUILDINGS

Achilles Karagiozis George Hadjisophocleous

ABSTRACT

Wind-driven rain is an important consideration in the hygrothermal performance of a building envelope. To date, very little work is available that provides field or laboratory wind-driven rain data to be used with moisture transport models. This information is a definite requirement as a boundary condition by the more sophisticated hygrothermal models before one can predict the hygrothermal performance of a building envelope.

In this paper, the wind-driven rain striking the exterior facade of a high-rise building is generated using a three-dimensional computational fluid dynamics (CFD) model that solves the airflow and particle tracking of the rain droplets around the building. One set of simulations was done using turbulence and velocity profiles for a building located in a suburban, open-country area. Four factors that govern wind-driven rain are investigated in this work: (a) upstream unobstructed wind conditions, (b) rainfall intensity, (c) probability distribution of raindrop sizes, and (d) local flow patterns around the building. These factors make wind-driven rain on a building facade very distinct. Simulations were carried out for three wind speeds of 5, 10, and 25 m/s; three rainfall intensities of 10, 25, and 50 mm/h; and one wind direction 0°, from the west face of the building. Nine simulations were conducted for the selected high-rise building.

The results show distinct wetting patterns on the top of the building that are parabolic in shape when the wind orientation is normal to the exterior facade surface. Indeed, twice the rain intensity is present at the upper top location of the high-rise building than the lower portion when a wind speed of 25 m/s is used. Wind speed was found to be the most critical factor influencing the amount of rain striking the exterior facade of the building. Results from these simulations are presented that demonstrate the effect of wind conditions and rain intensities on the wetting patterns on all wall building faces.

INTRODUCTION

In the past, building designers concentrated on making buildings more energy efficient and airtight. Hygrothermal performance and durability were not addressed properly, leading in some instances to major moisture-induced damage.

Durability of a building envelope system essentially depends on how the system responds to different external and internal environmental changes, such as pressure, sound, vibration, temperature, and moisture. In the interior, moisture can be generated by various sources and generally follows both daily and seasonal cycles. The exterior surface (facade) is constantly interacting with the ambient temperature, solar radiation, wind pressure, relative humidity, and wind-driven rain. Wind-driven rain is defined here as rain droplets carried along by wind having a characteristic angle with respect to the vertical. This paper presents results on wind-driven rain on a high-rise building's envelope performance.

Recently, a few sophisticated heat-air-moisture transport models (Karagiozis 1993; Salonvaara 1994; Pedersen 1990; Kieβl 1991) have appeared to predict the long-term hygrothermal behavior of building envelope systems. These models, to varying degrees of complexity, can handle vapor and liquid transport, crack flows, latent heat effects, and wind-driven rain. In a companion paper by Salonvaara and Karagiozis (1995), wind-driven rain was determined to be an important contributor to the total amount of moisture entering the structure. The instantaneous amount of moisture accumulation within the structure was found to increase threefold or more depending on the specific topographical location of the building. In these situations, where moisture accumulates at rather high levels, structural deterioration due to freeze-thaw cycles may occur. Wind-driven rain entering the facade of the structure accelerates the normal deterioration process and therefore reduces the service life of the building. Therefore, any short-term or long-term hygrothermal study on building envelopes requires the accurate prescription of wind-driven rain information as boundary condition inputs, especially when these studies lead to design guidelines. Wind-driven rain is a complex phenomenon itself, relatively unresearched and still not fully understood. Rain droplets with a wide range of

Achilles Karagiozis and **George Hadjisophocleous** are research officers at the National Research Council Canada, Institute for Research in Construction, Ottawa, Ont., Canada.

sizes are transported by wind that has a distinct three-dimensional behavior near buildings. The trajectory of the droplets is time dependent due to the effect of turbulence. Furthermore, rain droplet size distributions vary randomly with respect to time and space. For these reasons, the amount of rain striking the exterior surfaces of a building is unique to that building, as it depends on the local geometry of the building, topography around the building, wind speed, wind direction, rain intensity, and rain droplet distribution.

Knowledge available on wind-driven rain, albeit limited, has been predominantly determined by field experiments (Lacy 1951, 1965; Schwarz and Frank 1973; Hens and Mohamed 1994). Recently, however, investigations employing computational fluid dynamics (CFD) methods (Choi 1991, 1992; Wisse 1994) have appeared. Lacy (1965), a pioneer in the area of wind-driven rain, carried out extensive on-site measurements, and recently the British Code of Practice (BCP) (BSI 1992) presented an updated estimate method for driving rain. Wisse (1994) critically evaluated the assumptions involved in the estimate method of the BCP, compared it to measurements of Schwarz and Frank (1973), and found major disagreement. Wisse (1994) also predicted rain wetting patterns using a two-dimensional CFD approach. Hens and Mohamed (1994) experimentally measured driving rain striking a two-story school and compared it to driving rain calculation methods and found that the simplified theory approach (modification of BCP) overestimated the amount of driving rain by 25%. Choi presented two- (Choi 1992) and three-dimensional (Choi 1991) CFD results on wind-driven rain conditions and determined several rain intensity factors for stand-alone buildings. In these studies, however, a turbulent particle-tracking method for modeling rain droplet trajectories was not used. Furthermore, the flow and rain droplets were not fully coupled. This uncoupling between air and rain droplets may become critical at very high rain intensities. Preliminary laboratory investigations using wind tunnel methods have been performed by Surry et al. (1994). The authors showed higher wind-driven rain striking at the upper parts of the building model, thus confirming some of the previous field and computational results. High-rise buildings are exposed to harsher environmental conditions than those for low-rise buildings. The present study numerically examines wind-driven rain hitting the exterior surface of a stand-alone high-rise building. The influence of wind speed and rain intensity on the amount of rain striking the exterior surfaces of a high-rise building was investigated.

WIND-DRIVEN RAIN

Wind-driven-rain, as discussed above, is strongly affected by the local wind around a building. Rain droplets, in the absence of wind, fall down vertically under the influence of gravity. This would imply that the amount of rain hitting the walls of a building in the absence of wind will be theoretically zero. Near the vicinity of a building, raindrop trajectories are affected not only by the unobstructed wind flow but also by the particular flow distribution surrounding the building. Listed below are some of the important governing factors for the problem of wind-driven rain (Choi 1991):

- the upstream wind conditions, including the unobstructed wind velocity profile, turbulence intensity profile, and turbulence eddy length scale, as well as the ground surface roughness height;
- the local flow pattern around the building, which is related to the upstream wind conditions, the surface roughness of the building, the geometrical configuration of the building, and the surrounding conditions of the building;
- rainfall intensity; and
- the size distribution of the raindrops.

It is evident that each high-rise building will have its own distinct wetting pattern during a rainstorm. This implies that the present results on wind-driven rain depend on the local weather conditions and building geometry.

MODELING METHOD

Wind Flow Around the Buildings

The prediction of wind-driven rain distribution on high-rise buildings requires the determination of the local three-dimensional time-averaged velocities, velocity fluctuations, and the time-averaged pressures. The flow field around a bluff body, even for a simple cube, is very complicated. It includes a turbulent boundary layer, stagnation region, separation, reattachment, circulation, and von Karman's vortex sheets. The equations governing wind flow around buildings are the incompressible Navier-Stokes equations and the continuity equation. Closure to these equations is provided by various turbulence models, including the k-ε two-equation model, the algebraic second-moment closure model (ASM), and the large eddy simulation. Specific details about these models can be found in Rodi (1981), Launder and Spalding (1974), and Murakami (1992). The k-ε model is one of the most commonly used models in the field of wind engineering, and it has been adopted for this study.

Governing Equations for Turbulent Flow For incompressible turbulent flows, with the assumption that density fluctuations can be neglected, the mean form of the conservative equations of mass, momentum, and energy (x_j) can be written as follows:

Conservation of mass:

$$\frac{\partial}{\partial x_j}(\rho u_j) = 0 \tag{1}$$

Conservation of momentum:

$$\frac{\partial}{\partial t}(\rho u_i) + \frac{\partial}{\partial x_j}(\rho u_j u_i) = -\frac{\partial P}{\partial x_i} - \frac{\partial}{\partial x_j}(\tau_{ij} + \rho\overline{u'_i u'_j}) + S_{u_i} \quad (2)$$

where

u_i = velocities in the x_i directions,
ρ = density of the fluid,
P = static pressure,
τ_{ij} = viscous stress tensor, and
S_{u_i} = additional source terms.

All these variables are mean flow quantities (time averaging) and u_i' represents the fluctuating part.

The term $\rho\overline{u'_i u'_j}$, which appears in the momentum equation (Equation 2), is defined as the turbulent Reynolds stresses. These terms are not expressible in terms of the mean flow variables; therefore, they must be related to known quantities via a turbulence model before solving the above equations. The k-ε model employed in this study is described below. Local values of the turbulent kinetic energy, k, and its dissipation rate ε are obtained from the solution of the following semi-empirical equations:

$$\rho\frac{Dk}{Dt} = \frac{\partial}{\partial x_j}\left(\Gamma_k\frac{\partial k}{\partial x_j}\right) + P_k - \rho\varepsilon \quad (3)$$

$$\rho\frac{D\varepsilon}{Dt} = \frac{\partial}{\partial x_j}\left(\Gamma_\varepsilon\frac{\partial \varepsilon}{\partial x_j}\right) + \frac{\varepsilon}{k}(c_{\varepsilon_1}P_k - c_{\varepsilon_2}\rho\varepsilon) \quad (4)$$

where

$k = \overline{u'_i u'_i}/2$ = turbulent kinetic energy,
$\Gamma_k, \Gamma_\varepsilon$ = diffusion coefficients, and $\Gamma_k = \mu + \mu_t/\sigma_k$, $\Gamma_\varepsilon = \mu + \mu_t/\sigma_\varepsilon$,
$P_k = -\rho\overline{u'_i u'_j}\partial u_i/\partial x_j$ = production of k,
$\varepsilon = \frac{\mu}{\rho}\overline{(\partial u'_i/\partial x'_j)^2}$ = dissipation of k,
μ_t = turbulent eddy viscosity,
μ = molecular viscosity, and

turbulence model constants are listed as

$c_{\varepsilon 1}$ = 1.44,
$c_{\varepsilon 2}$ = 1.92,
σ_k = 1.0,
σ_ε = 1.3,
c_μ = 0.09, and
Pr_t = 0.9.

For this study the CFD code TASCflow (ASC 1993) was used.

RAIN DROPLET MODELING

In this section, information is presented regarding the size distribution of rain droplets, followed by a discussion of the three-dimensional Lagrangian turbulent particle-tracking method employed.

Size Distribution of Raindrops

Calculation of the amount of rainfall impinging on the building facades requires knowledge of the size distribution of raindrops in a particular storm. Best (1950) carried out an extensive experimental study of rain droplet size distributions and their relationship with rainfall intensity. The results of his study can be summarized by the following simple correlation:

$$F(d) = 1 - \exp[-d/a]^n \quad (5)$$

$$a = AI^P \quad (6)$$

$$W = CI^r \quad (7)$$

where F is the fraction of liquid water in the air composed of drops with a diameter less than d, I is the rate or intensity of rainfall, and W is the amount of liquid water per unit volume of air. A, c, p, r, and n are constants. If d is measured in mm, I in mm/h, and W in mm^3/m^3, the mean values of A, c, p, r, and n are 1.30, 67, 0.232, 0.846, and 2.25, respectively.

Rain Trajectories Using the Lagrangian Particle-Tracking Method

Many engineering problems, such as wind-driven rain, involve the study of mixtures containing a continuous phase that exhibits fluid properties and a dispersed phase that is discretely distributed in the fluid. With the dispersed phase, there is no continuum, the phase can be considered as a set of individual discrete rain droplet particles, and each particle interacts with the fluid and other particles discretely. A Lagrangian tracking model can be used to predict the behavior of the dispersed phase. The Lagrangian tracking method tracks several individual rain droplets through the flow field and involves the integration of particle paths through the discretized domain. Individual rain droplets are tracked from their injection point until they escape the domain or some integration limit criterion is met. The rain droplets are assumed to have a spherical shape and their density is much greater than the air fluid density. The governing equation of motion for rain droplets, employing the above assumptions, can be written as

$$\frac{\pi d^3}{6}\frac{du_p}{dt} = \frac{3\pi\mu d}{C_{cor}}(u_f - u_p) + F_e \quad (8)$$

where d is the rain droplet diameter, u is the velocity, and F_e is an external potential force. The subscript f refers to the fluid and the subscript p refers to the rain droplet. For a moderate rain droplet, the Reynolds number $0.01 < \mathrm{Re}_p < 260$, the drag correction, introduced to

account for experimental results on viscous drag of a solid sphere, is

$$C_{cor} = 1 + 0.1315\,(\mathrm{Re}_p)^{0.82-0.05a} \quad \mathrm{Re}_p < 20 \qquad (9)$$

$$= 1 + 0.1935\,(\mathrm{Re}_p)^{0.6305} \quad \mathrm{Re}_p > 20 \qquad (10)$$

where $\alpha = \log \mathrm{Re}_p$ and the particle Reynolds number is calculated from

$$\mathrm{Re}_p = \rho_f |u_f - u_p| \frac{d}{\mu}. \qquad (11)$$

BUILDING STRUCTURES AND COMPUTATIONAL DOMAIN

In this study, a high-rise building located in an area sparsely populated by low-rise buildings is considered. This building will be referred to as the open-country case and is shown in Figure 1a. The width of the high-rise building, defined as *h*, is used as the measuring unit for the geometry of the domain. The simulation domain, with a downstream length of 16 *h*, an upstream length of 16 *h*, a lateral width of 4 *h* on each side, and a vertical height of 10 *h* was discretized. The computational domain was extended far before and after the building structure to accommodate far-field effects. To avoid using a highly nonuniform spacing grid system, grid embedding close to the high-rise building was employed. For the open-country case, a building model of $1 \times 2 \times 1$ *h* was used with $81 \times 31 \times 31$ control volumes in the grid embedding zone and $36 \times 11 \times 10$ control volumes outside the embedding zone in the x, y, and z directions, respectively. Figure 1b displays the part of the overall grid in both the x-y and x-z planes.

BOUNDARY CONDITIONS

Upstream Boundary

Wind velocity and turbulence intensity profiles for the upstream inlet were assigned values as given by Baskaran (1992), suburban open-country conditions.

Upper Faces of the Computational Domain

The upper faces of the computational domain are defined as a slip-wall with zero shear stresses.

Downstream Boundary and Side Faces of the Computational Domain

These boundaries are set to be pressure-specified openings. Pressures outside the boundaries were assumed to be zero.

High-Rise Wall Boundary

The building's walls and ground are assumed to be rough surfaces. For the high-rise walls and ground, an equivalent sand-grain roughness height of 0.1 m and 0.03 m, respectively, are used in the simulations.

Rain Droplet Tracking

In this study, the rain droplets are divided into a number of groups according to their size. A maximum of 18 groups, depending on the rain intensity, with approximately 3,000 droplets in each group, were injected from different planes of the domain. The droplet termi-

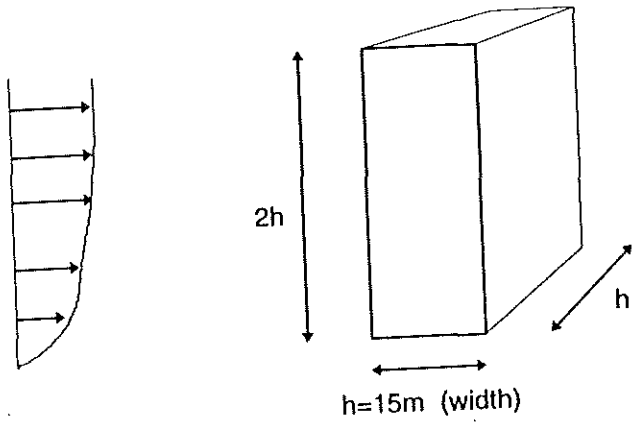

Figure 1a Geometry for the open country high-rise building.

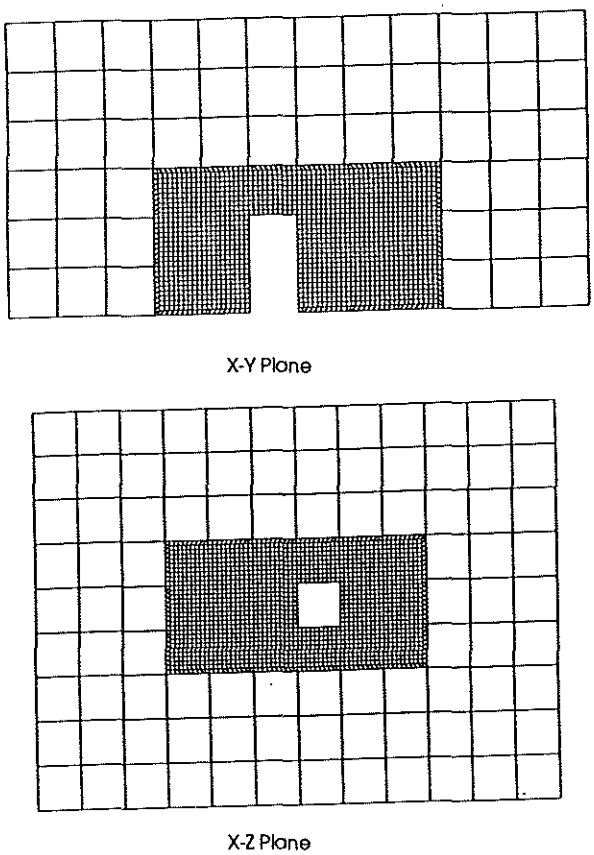

Figure 1b Grid geometry for the open country high-rise building.

nal velocities and the mass flow rate for each group were defined prior to the simulations at the injection joints.

SIMULATION CASES

In this study, the water mass flow distributions due to wind-driven rainwater on the four walls of the high-rise building were computed for three different wind speeds, one wind angle, and three rain intensities as follows:

- wind speed (at gradient height): 5 m/s, 10 m/s, 25 m/s;
- wind directions (with respect to west): 0°; and
- rain intensities: 10 mm/h, 25 mm/h, 50 mm/h.

The rain intensities that were chosen are representative of the rain patterns found in most of the habitable areas of Canada.

DISCUSSION OF RESULTS

In Figure 2, wind velocity distributions are displayed around the high-rise building. The velocity field at the center (X-Y) plane of the building is shown for a gradient height velocity of 5 m/s. The flow around the high-rise building clearly indicates that high-velocity gradients surround the building. Furthermore, since rain droplets are dispersed in the continuous air phase, the local acceleration and deceleration create rapidly changing transport forces on each rain droplet. Figures 3a and 3b show a limited number of wind-driven rain trajectories at two different rain droplet diameters of 0.5 and 5.0 mm. Trajectory results are shown for the same X-Y plane as the one used for the velocity distributions. While the figures depict trajectories with fairly straight lines, in a three-dimensional presentation this is far from true. The influence of droplet diameter size on wetting behavior due to wind-driven rain is demonstrated to be very important. These figures, at the gradient height velocity of 5 m/s, show that the velocity field has a greater influence on the droplet trajectories for small-diameter particles than for droplets of much larger (5.0 mm) diameters. For the 5.0-mm-diameter rain droplet sizes, the droplet trajectories become more parallel to each other. In Figure 4, the rain droplet trajectories are shown for all droplet sizes for a wind speed of 25 m/s. Here the additional influence of higher wind speeds is clearly demonstrated. Figure 5 shows the effect of wall orientation (west-, east-, and north-facing) on the amount of rain each wall receives when employing a rain intensity of 10 mm/h and a wind speed of 10 m/s. The south wall receives a similar amount of rain as the north wall but is not shown here.

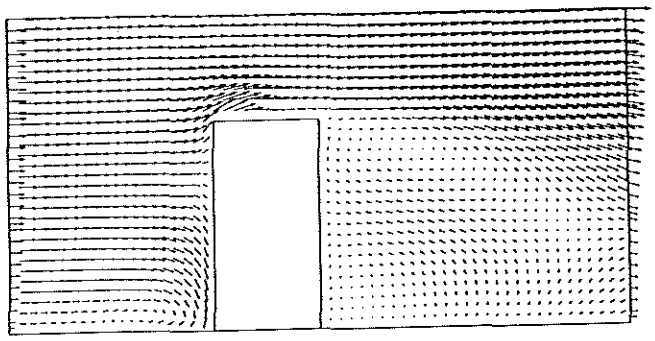

Figure 2 Open country velocity distribution for the symmetric X-Y plane using a gradient height velocity of 5 m/s.

The ratio *Iwall/Irain* is defined here as the intensity of rain that strikes the wall over the normal rainfall intensity. A distinct vertical wetting pattern of distribution from the bottom to the top of the building is present. The west face, which is normal to the wind speed, receives more wind-driven rain, and the upper top area of the building receives the highest amount of rain for all faces. Irregularities in the trend, as we move from the bottom of the building to the top, are due to the randomness of the turbulent Lagrangian particle-tracking method used. Figure 6 shows the rain intensity factors (*Iwall/Irain*) as a function of rain intensities of 10, 25, and 50 mm/h for a west-facing wall. Results indicate that rain intensity has a minor effect on the wind-driven rain distribution as a function of height. Finally, Figure 7 illustrates the significant effect of wind speed on the rain

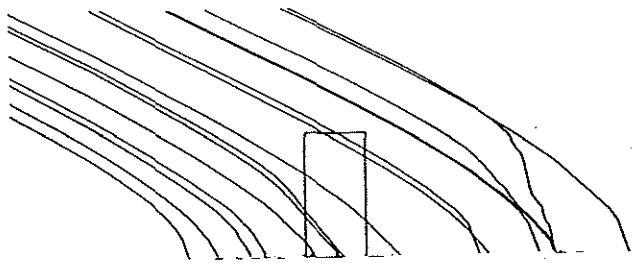

Figure 3a Trajectories for the 0.5 mm diameter rain droplets at 5 m/s gradient height wind speed (open country case).

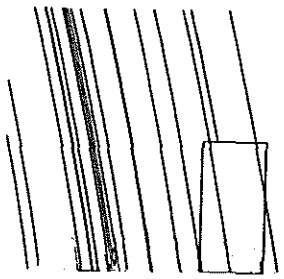

Figure 3b Trajectories for the 0.5 mm diameter rain droplets at 5 m/s gradient height wind speed (open country case).

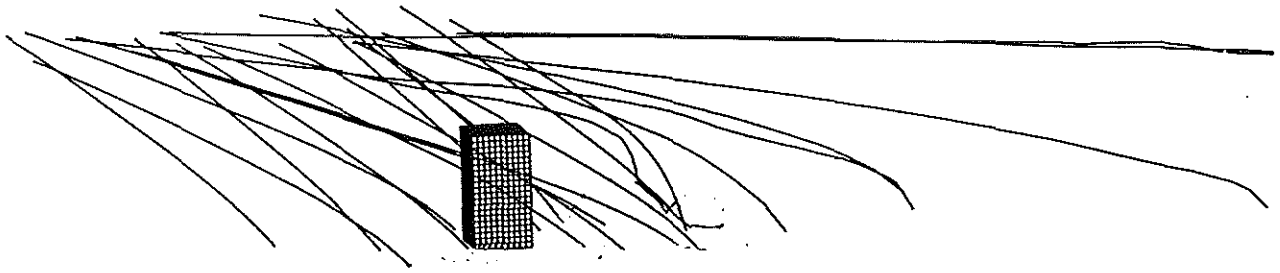

Figure 4 Three-dimensional trajectories for rain droplets using a wind velocity of 25 m/s and a rain intensity of 25 mm/h.

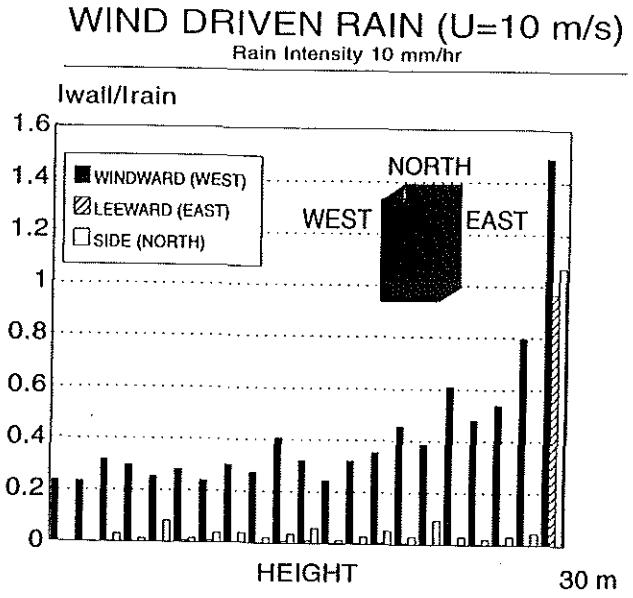

Figure 5 Wind-driven rain intensity factors for the west, east, and north faces of the high-rise building, using U = 10 m/s, and Irain = 10 mm/h.

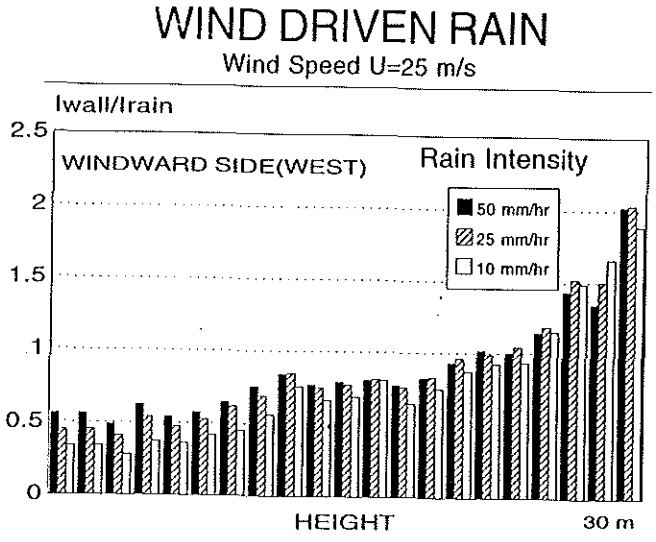

Figure 6 Wind-driven rain intensity factors for the west facing wall as a function of rain intensities, using U = 25 m/s.

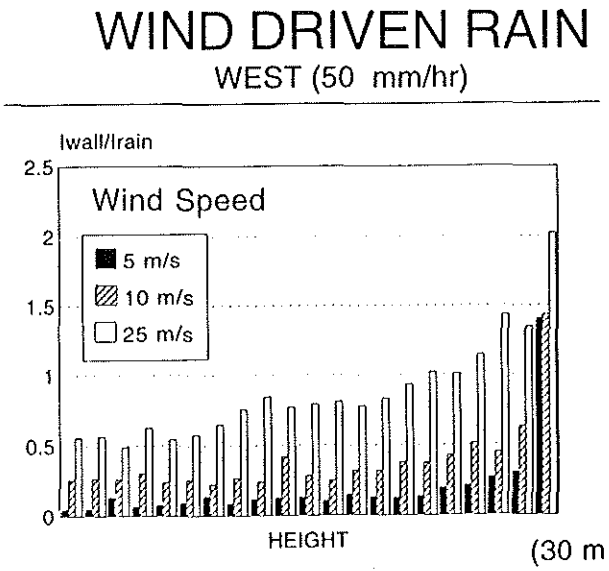

Figure 7 Wind-driven rain intensity factors for the west facing wall as a function of wind speed, using Irain = 50 mm/h.

intensity factor *Iwall/Irain*, again on the west face of the building using a rain intensity of 25 mm/h.

CONCLUSIONS

A CFD method for predicting the wetting patterns on high-rise structures during wind-driven rain is presented in this paper. For all cases, the amount of wind-driven rain striking the building increases from bottom to top. The results show that the downstream side (east is the case considered) of the wall receives no rain except near the top due to the wind-induced recirculation in that region. This investigation found that at a wind speed of 25 m/s, the upper top areas of the high-rise building received twice the horizontal rain intensities. The results show that the rainfall intensity does not significantly affect the wetting pattern of the building walls. Higher wind speeds, however, were found to significantly increase the amount of water received on the building facade. The higher the wind speed, the higher the amount of water received.

Information generated using this complex three-dimensional flow and turbulent particle-tracking ap-

proach is essential for accurate hygrothermal modeling. The amount of rain hitting the exterior facades of a building must be incorporated into hygrothermal models so as to account for liquid transport at the surfaces. Indeed, extending the scope of this work with the issue of water rundown is also important. The analysis of durability issues with respect to the hygrothermal performance can only start when models are equipped with methods of incorporating driving rain.

Future work will focus on considering different wind speed orientations, building obstructions, and other factors that influence wind flows around a building with the objective of developing simple correlations that can be used in design guidelines. Due to the extremely high computation time (CPU) requirements and complex transport mechanisms involved in wind-driven rain, an international collaborative effort could allow rapid progress in this area.

ACKNOWLEDGMENTS

The authors gratefully acknowledge the assistance of Shu Cao in the computations. This work was partially supported by Canada Mortgage and Housing Corporation (CMHC) under a joint research project. CMHC's support is greatly appreciated.

REFERENCES

ASC. 1993. *Theory documentation for TASCflow,* version 2.2. Waterloo, Ont.: Advanced Scientific Computing Ltd.

Baskaran, A. 1992. Review of design guidelines for pressure equalized rainscreen walls. NRC Internal Report No. 629.

Best, A.C. 1950. The size distribution of raindrops. *Quarterly Journal of Royal Meteorology Society* 76: 16-36.

BSI. 1992. British standard code of practice for assessing the exposure of walls to wind-driven rain. BS 8104. London: British Standards Institution.

Choi, E.C.C. 1991. Numerical simulation of wind-driven rain falling onto a 2-D building. In *Computational Mechanics,* Cheung, Lee, and Leung, eds., pp. 1721-1727. Rotterdam: Balkema.

Choi, E.C.C. 1992. Simulation of wind-driven rain around a building. *Journal of Wind Engineering* 52: 60-65.

Hens, H., and F.A. Mohamed. 1994. Preliminary results on driving rain estimation. International Energy Agency, Annex 24, T2-B-94/02.

Karagiozis, A. 1993. Overview of the 2-D hygrothermal heat-moisture transport model LATENITE. Internal IRC/BPL Report.

Karagiozis, A., and M. Salonvaara. 1995. The effect of waterproof coating on hygrothermal performance of a high-rise wall structure. *BETTEC95, Thermal Envelopes VI,* Clearwater, Fla.

Kießl, H. 1991. Classification of WUFIZ. IEA Annex 24.

Lacy, R.E. 1951. Distribution of rainfall round a house. *Meteorol. Magazine* 80: 184-189.

Lacy, R.E. 1965. Driving rain maps on the onslaught of rain on buildings. Current Paper No. 54. Garston, U.K.: Building Research Station.

Launder, B.E., and D.B. Spalding. 1974. The numerical computation of turbulent flows. *Comput. Meth. Apl. Mech. Eng.* 3: 269.

Murakami, S. 1992. Comparison of various turbulence models applied to a bluff body. First International Symposium on Computational Wind Engineering, *Journal of Wind Engineering,* no. 52.

Pedersen, C.R. 1990. Combined heat and moisture transport in building constructions. Ph.D. Thesis, Report 214. Thermal Insulation Laboratory, Technical University of Denmark.

Rodi, W. 1981. Examples of turbulence models for incompressible flows. *AIAA J.* 20: 267.

Salonvaara, H.M. 1994. TRAMTO2. Finland: VTT.

Schwarz, B., and W. Frank. 1973. Schlagregen, Berichte aus der Bauforschung, Heft 86, Berlin.

Surry, D., D.R. Inculet, P.F. Skerlj, J.X. Lin, and A.G. Davenport. 1994. Wind, rain and the building envelope. Wind, Rain and the Building Envelope Seminar, University of Western Ontario, May 16-17.

Wisse, J.A. 1994. Driving rain, a numerical study. 9th Symposium for Building Physics and Building Climatology, 14-16 September, Dresden.